Signal Processing 93 (2013) 1317–1327

Contents lists available at SciVerse ScienceDirect

Signal Processing

journal homepage: www.elsevier.com/locate/sigpro

Time of arrival and power delay profile estimation for IR-UWB systems ☆

Fang Shang*, Benoit Champagne, Ioannis Psaromiligkos

Department of Electrical and Computer Engineering, McGill University, Montreal, Quebec, Canada, H3A 2A7

ARTICLE INFO

Article history:
Received 3 April 2012
Received in revised form
24 October 2012
Accepted 2 November 2012
Available online 29 November 2012

Keywords:
Ultra-wideband (UWB) pulse signals
Time of arrival (TOA) estimation
Average power delay profile (APDP)
Source localization
Radio frequency identification (RFID)

ABSTRACT

In time of arrival (TOA) estimation of received ultra-wideband (UWB) pulses, traditional maximum likelihood (ML) and generalized likelihood estimators become impractical because they require sampling at the Nyquist rate. Sub-Nyquist ML-based TOA estimation currently assumes *a priori* knowledge of the UWB channels in the form of the average power delay profile (APDP). In this paper, instead of assuming a known APDP, we propose and investigate a joint estimator of the TOA and the APDP. We assume a multi-cluster parametric APDP model and estimate its parameters via a least-squares approach; the estimated APDP is then used in connection with a ML criterion to obtain the TOA estimate. The proposed method has a low sampling rate requirement and is well-suited for real-time implementation. Simulation results show that it can achieve improved accuracy in practical UWB TOA estimation scenarios, when compared to other competing approaches.

1. Introduction

In the past few years, applications of localization and tracking algorithms in wireless sensor networks (WSN) and radio frequency identification (RFID) have received considerable attention. RFID-based localization allows an object or person to be identified and located using a radio wave transmission [1] from a RFID transmitter (tag) to the multiple RFID receivers (tag readers). The spatial coordinates of the RFID tag are calculated by triangulation based on range measurements as obtained from, e.g., time of arrival (TOA) estimation of the received signals at the tag readers [2]. Impulse radio (IR) ultra-wideband (UWB) signals are particularly well suited for this task, as they can provide very accurate TOA estimates which, in turn, can lead to localization within an order of a few centimeters [3].

Traditionally, TOA estimation is performed by using a correlation or matched filter (MF) receiver, where the received noisy signal is matched to a time-shifted replica of the undistorted transmitted pulse waveform. The TOA estimate is then obtained as the time shift corresponding to the peak value of the squared output of the MF. In the case of a single path radio channel, and under low noise conditions, this method provides good estimates of the unknown delay, which is equal to the propagation time between the tag and the tag reader (assuming there is no synchronization error). However, these ideal conditions are rarely met in practical applications of UWB signals to RFID localization [4], where the typical radio channel exhibits a complex multipath structure [5].

In particular, due to the multipath propagation, it is very likely that the strongest multipath component will not correspond to the first arrival path [6]. Therefore, MF based methods are in general not applicable to TOA estimation of UWB signals. A maximum likelihood (ML) TOA estimator was derived in [7] with explicit consideration of multipath propagation. Its performance was shown to closely approach the Cramer-Rao bound (CRB) at high

☆ This work was supported in part by the Fonds québécois de la recherche sur la nature et les technologies.

* Corresponding author. Tel.: +1 514 562 3828.
E-mail address: fang.shang@mail.mcgill.ca (F. Shang).

0165-1684/$ - see front matter © 2012 Elsevier B.V. All rights reserved.
http://dx.doi.org/10.1016/j.sigpro.2012.11.006

signal-to-noise ratios (SNRs). However, the excessive computational cost associated with the search over the multi-dimensional delay and gain space, combined with the high sampling rate requirement, render this joint estimator impractical for UWB channels with a large number of multipaths, as it is well recognized in the literature [3,8]. To reduce complexity, the generalized maximum likelihood (GML) estimator was proposed in [9]. Under the assumption that the strongest path has been correctly acquired, this estimator obtains the desired TOA as the location of smallest delay found to be above a predetermined threshold during a backward search starting from the strongest path location.

Although the previously mentioned ML-based approaches can achieve good TOA estimation accuracy, the requirement of sampling the received signals at the Nyquist rate makes them impractical due to the prohibitive implementation costs. Consequently, TOA estimation approaches with lower sampling rate requirements have gained significant interest in the recent years. Although the performance of the sub-Nyquist estimators is not as good as that of the Nyquist ones, their low computational complexity makes them attractive for low-cost ranging applications. In particular, low-complexity estimators based on the energy detection (ED) receiver [10–12] have become quite popular. Within this class, Gezici et al. [10] propose a two-step approach, in which TOA estimation is performed by first obtaining a coarse TOA estimate based on ED, and then refining the estimate via hypothesis testing. The performance of low-sampling rate MF and ED for TOA estimation based on thresholding is analyzed and compared in [11]. Two new Bayesian TOA estimators that rely on the overall energy profile available at the output of the ED are proposed in [12]. A main disadvantage of ED-based estimators is that they may suffer greatly from noise and their performance thus degrades rapidly at low SNR. ML estimators based on sub-Nyquist sampling models have also been proposed, such as the maximum energy sum selection (MESS) and its weighted (W-MESS) and double-weighted (DW-MESS) versions [13]. In [14], ML timing estimation with sub-sampling is proposed under the assumptions of normally distributed channel impulse response and known power delay profile.

These sub-Nyquist sampling ML estimators can achieve good estimation accuracy, but to function properly, they generally require *a priori* information about the channel, in the form of the average power delay profile (APDP), which should be estimated beforehand. As we have been able to verify, a lack of adequate information about the APDP can significantly deteriorate the performance of these estimators. Besides its application in ML-based TOA estimation, the APDP is an important characteristic of the UWB channel in its own right. Indeed, it can provide useful information about the characteristics of the multipath radio channel, including the presence of dominant scatterers in the vicinity of the RFID transmitter as well as the reflection/absorption properties of the surrounding environment. Despite its importance, the estimation of the ADPD from a statistical signal processing perspective has not yet been extensively explored.

In this work, we propose to jointly estimate the APDP of the UWB channel, along with the desired TOA of the IR signal at sub-Nyquist sampling rate. To this end, and motivated by the work of the IEEE 802.15.4a Task Group on standard channel models for IR-UWB systems [15], we adopt a multiple cluster parametric model for the APDP. The parameters of this model include the clusters' arrival times, peak power levels and decay rates which, together with the unknown TOA, define the unknown parameter vector subject to estimation. We first derive the likelihood function of the observed data for the complete set of unknown parameters. To simplify the multi-dimensional search, we consider a sub-optimal scheme in which the APDP parameters are first estimated via a least-squares approach. The resulting APDP is then used to find the TOA estimate via the ML criterion through a one-dimensional search at the chip level (sub-Nyquist). We also derive the CRB for joint unbiased estimators of the APDP parameters and TOA. Through numerical simulations of IR-UWB signal propagation in realistic multipath UWB channels, the proposed joint estimator is shown to produce accurate estimates of the TOA *and* the APDP parameters. The newly obtained APDP estimate can also be used in other existing sub-Nyquist estimators which need this information beforehand. Using the same chip sampling rate at the receiver, we show that the proposed joint TOA estimator outperforms the previous ones as it can achieve a finer accuracy in practical UWB TOA estimation scenarios. The proposed method has reasonable complexity and is well-suited for real-time implementation.

The remainder of this paper is organized as follows. Section 2 gives a description of the system model. The proposed method for joint TOA and APDP estimation is derived in Section 3 while in Section 4, the CRB for joint estimation of these parameters is derived. Performance comparisons of the proposed method to other benchmark approaches are presented and discussed in Section 5. Finally, a summary and conclusion are given in Section 6.

Regarding notations: A baseband signal model is assumed so that, unless otherwise indicated, all signals and physical quantities of interest are real-valued. Bold font is used to represent vectors and matrices. Superscript T is used to denote matrix transpose. $\boldsymbol{I}$ denotes an identity matrix of appropriate dimension. Finally, $E[\cdot]$ stands for expectation.

2. System model

We consider a RFID-based location system in which the tag transmits a time-hopping (TH) IR-UWB signal, $s(t)$, where t denotes time. TOA estimation is typically performed during the preamble section of a ranging packet. As described by the IEEE 802.15.4a standard, the preamble can contain a large number of symbols (e.g., up to 4096) [16]. To improve processing gain and suppress noise, averaging over the preamble symbols is a very common operation [3,17]. The signal $s(t)$ consists of N_f consecutive frames of duration T_f that amount to a total observation interval $T_o = N_f T_f$. In turn, each frame is divided into N_c consecutive chips of equal duration T_c, so that $T_f = N_c T_c$. Within the jth frame, $j = 0,1,\ldots,N_f-1$, a single IR-UWB pulse $w(t)$ is transmitted with a time offset of $c_j T_c$ relative to the beginning of the frame, where $c_j \in \{0,\ldots,N_c-1\}$ denotes the TH sequence. We assume that the UWB pulse waveform $w(t)$ has finite duration T_c, i.e., $w(t) = 0$ for $t \le 0$

and for $t \geq T_c$. In addition, the pulse transmitted within the jth frame is affected by a polarity code, $d_j \in \{+1,-1\}$, used for spectrum smoothing [4]. A data aided approach is employed in this work in which a known training sequence (i.e., all zero) is used, which is very common in this application, e.g., [10,18].

Accordingly, the transmitted signal can be expressed in mathematical form as

$$s(t) = \sum_{j=0}^{N_f-1} d_j \sqrt{E_p} w(t - jT_f - c_j T_c), \quad 0 \leq t \leq T_o \tag{1}$$

where $E_p > 0$ will denote the transmitted energy per pulse. In practice, both sequences c_j and d_j are known to the receiver. In this work, since we consider the single user case, no TH code will be used; without loss in generality, we therefore set $c_j = 0 \forall j$.

The transmitted UWB signal $s(t)$ propagates over a multipath channel before reaching the tag reader. A tapped delay line model is employed to characterize the UWB multipath channel, as in [10,19]. Assuming a tap spacing of T_c, this model represents the impulse response $h(t)$ of the channel as the sum of scaled and delayed impulses[1]

$$h(t) = \sum_{l=0}^{L-1} a_l \delta(t - \tau_l) \tag{2}$$

where $\delta(\cdot)$ is the Dirac delta function, a_l is a zero-mean random variable representing the amplitude of the lth multipath component, $\tau_l = lT_c + \tau_0$ is the propagation time delay of the lth multipath, $\tau_0 > 0$ is the deterministic but unknown delay of the first path, and L is the number of time-resolvable multipaths. According to (2), the channel delay spread is given by $\tau_{ds} = LT_c$. Here, the focus is on sub-Nyquist TOA resolution and hence we assume that τ_o is a multiple of the chip duration, i.e., $\tau_0 = DT_c$ where D is an integer [10]. This approach reduces the search complexity of the delay estimation; yet, as will be illustrated in Section 5, our proposed algorithm can be applied with arbitrary values of τ_0.

Since the tapped delay line model is based on the use of resolvable time delay bins, the temporal correlation coefficients between adjacent tap amplitudes are very small and can be neglected according to the previous studies [20,21,14]. Therefore, the channel tap vector, defined as $\boldsymbol{h} = [a_0, \ldots, a_{L-1}]^T$, has zero mean and covariance matrix

$$\boldsymbol{R}_h = E[\boldsymbol{h}\boldsymbol{h}^T] = \begin{bmatrix} P_0 & 0 & \ldots & 0 \\ 0 & P_1 & & \vdots \\ \vdots & & \ddots & 0 \\ 0 & \ldots & 0 & P_{L-1} \end{bmatrix} \tag{3}$$

where the sequence of the diagonal entries, $P_l = E[a_l^2]$, for $l = 0, \ldots, L-1$, constitutes the average power delay profile (APDP) of the channel.

The UWB channel model proposed by the IEEE 802.15.4a task group is based on the modified Saleh–Valenzuela model [15], where each channel tap amplitude

[1] The pulse distortion on each multipath component, due to the fine (time-unresolvable) structure of the channel, is ignored for simplicity.

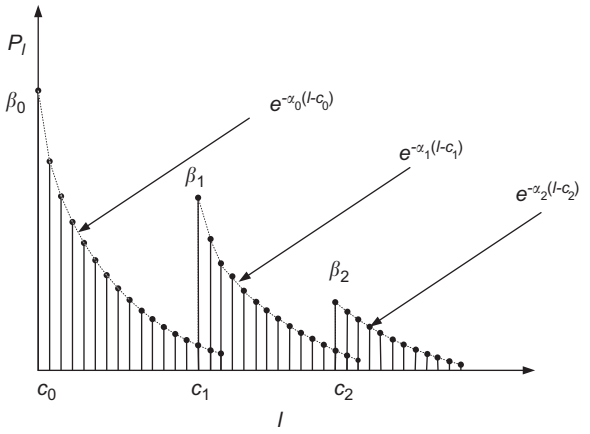

Fig. 1. APDP in Saleh–Valenzuela model.

a_l follows a Nakagami distribution, with the APDP conforming to the doubly exponential decay model with Poisson inter-arrival times. For mathematical convenience, we consider a simplified version of this model in which the amplitudes of the resolvable multipaths in (2) follow a Gaussian distribution, with the associated APDP expressed as a sum of multiple, exponentially decaying clusters, as follows (see also Fig. 1):

$$P_l = \sum_{k=0}^{C-1} \beta_k e^{-\alpha_k(l-c_k)} u(l-c_k), \quad l = 0, \ldots L-1 \tag{4}$$

where C is the total number of clusters, $k \in \{0, \ldots, C-1\}$ is the cluster index, the non-negative parameters β_k, α_k and c_k represent the peak power level, exponential decay rate and start time (i.e., arrival time of the first path) of the kth cluster, respectively, and $u(l)$ denotes the unit step function (i.e., $u(l) = 1$ for $l \geq 0$ and 0 otherwise). We note that c_k represents the arrival delay of the first path within the kth cluster, relative to the first arrival delay D. Therefore $c_0 = 0$ and $c_k < c_{k+1}$.

The parameters of this APDP model, depend on the characteristics of the UWB radio propagation environment. We emphasize that the modeling simplifications are made purely for the sake of developing a mathematically tractable algorithm; in our simulation experiments in Section 5, the resulting algorithm will be shown to perform adequately when applied to more accurate UWB channel models that comply with the IEEE 802.15.4a standard.

After multipath propagation, the received UWB signal at the tag reader can be expressed as

$$r(t) = \sum_{l=0}^{L-1} a_l s(t - \tau_l) + n(t), \quad 0 \leq t \leq T_o \tag{5}$$

where $n(t)$ is an additive noise term modeled as a white Gaussian process. We assume that T_f is sufficiently large such that there is no interframe interference, that is, the scaled and delayed replicas of the transmitted pulse during the jth frame are received during that frame, which is possible if $0 \leq \tau_0 \leq \tau_{max}$ where the maximum delay satisfies $0 \leq \tau_{max} \leq T_f - \tau_{ds}$. In practice, this assumption is

well justified since the transmitted pulse signal has a low duty cycle. Specifically, the pulse repetition period is of the order of 1 μs while the delay spread of a typical indoor channel is of the order of a few 100 ns. Nevertheless, the effect of a small amount of inter-frame interference (IFI) is further considered in our simulation experiments (see Section 5). Under this assumption, it follows from (1) and (5) that

$$r(jT_f+t)=d_j\sqrt{E_p}\sum_{l=0}^{L-1}a_l w(t-\tau_l)+n(jT_f+t),\quad 0\le t<T_f. \tag{6}$$

To derive the TOA estimator, an equivalent discrete-time version of the signal model will be used. We first consider uniform sampling at the rate $1/T_s$, where $T_s\le 1/2B$ and B is the bandwidth of the transmitted IR signal. Let $M=T_c/T_s$ be an integer, so that each frame is represented by MN_c samples and let $\boldsymbol{r}_j=[r(jT_f),\ldots,r(jT_f+(MN_c-1)T_s)]^T$ denote the column vector of discrete-time noisy signal samples of the jth frame. Similarly, the IR pulse $w(t)$ can be represented by the column vector $\boldsymbol{w}=[w(0),\ldots,w((M-1)T_s)]^T$ and we let $\boldsymbol{w}$ have unit energy. We emphasize that the sampling period T_s mentioned here is used only to analyze the discrete-time system model; in the end, the proposed estimator will only require the evaluation of the likelihood function at the sub-Nyquist chip rate of $1/T_c$ (see Section 3).

Making use of (6), the vector of received signal samples $\boldsymbol{r}_j$ in the jth frame can be written as

$$\boldsymbol{r}_j=d_j\sqrt{E_p}\boldsymbol{W}\boldsymbol{h}+\boldsymbol{n}_j \tag{7}$$

where $\boldsymbol{W}=[\boldsymbol{w}_D,\boldsymbol{w}_{D+1},\ldots,\boldsymbol{w}_{D+L-1}]$ is a $MN_c\times L$ matrix with columns

$$\boldsymbol{w}_d=\left[\underbrace{0,\ldots,0}_{dM},\ \boldsymbol{w}^T,\ \underbrace{0,\ldots,0}_{MN_c-M-dM}\right]^T \tag{8}$$

for $d\in\{D,D+1,\ldots,D+L-1\}$, and $\boldsymbol{n}_j$ is the discrete-time vector representation of the noise $n(t)$ in the jth frame with zero-mean and covariance matrix $\sigma_n^2\boldsymbol{I}$.

Given the set of observations $\boldsymbol{r}_j$, for $j\in\{0,\ldots,N_f-1\}$ and the knowledge that the UWB channel's APDP can be described as in model (4), our aim is to develop estimators for the unknown integer delay, D, and the modeling parameters of the APDP, that is, the number of clusters C, and the individual clusters' parameters α_k, β_k and c_k for $k\in\{0,\ldots,C-1\}$. In the absence of interframe interference, D is limited to the range $0\le D\le D_{max}=N_c-L$. The cluster parameters α_k and β_k are positive real numbers, and the associated shift parameters c_k are non-negative integers.

3. Joint estimation of APDP and TOA

In this section, we develop a novel approach for jointly estimating the unknown integer delay D and the parameters of the APDP. We first derive the log-likelihood function (LLF) for the joint estimation problem, based on the above modeling assumptions. To avoid the computational complexity of maximizing the likelihood function by searching over the complete parameter space, we propose a sub-optimal approach in which the APDP parameters are estimated via least-squares fitting using the parametric model in (4). The APDP estimates so obtained are substituted back into the LLF, which is finally maximized to obtain the desired delay estimate D.

3.1. Log-likelihood function derivation

Since the channel tap vector $\boldsymbol{h}$ and the additive noise vector $\boldsymbol{n}_j$ are independent Gaussian with zero-mean, it immediately follows from (7) that the vector of observations in the jth frame, $\boldsymbol{r}_j$, is also the Gaussian with zero-mean and covariance matrix

$$\boldsymbol{R}_{\boldsymbol{r}_j}=E[\boldsymbol{r}_j\boldsymbol{r}_j^T]=E_p\boldsymbol{W}\boldsymbol{R}_h\boldsymbol{W}^T+\sigma_n^2\boldsymbol{I} \tag{9}$$

where $\boldsymbol{R}_h$ is given by (3). In addition, because of the white noise assumption, the covariance matrix between observation vectors in different frames is simply

$$\boldsymbol{R}_{\boldsymbol{r}_i\boldsymbol{r}_j}=E[\boldsymbol{r}_i\boldsymbol{r}_j^T]=d_id_jE_p\boldsymbol{W}\boldsymbol{R}_h\boldsymbol{W}^T \tag{10}$$

Therefore, the covariance matrix of the complete received signal vector within the observation time $T_o=N_fT_f$ represented by $\boldsymbol{r}=[\boldsymbol{r}_0^T,\ldots,\boldsymbol{r}_{N_f-1}^T]^T$, can be described as the following block matrix

$$\boldsymbol{R}_r=E_p\boldsymbol{W}_r\boldsymbol{R}_h\boldsymbol{W}_r^T+\sigma_n^2\boldsymbol{I} \tag{11}$$

where $\boldsymbol{W}_r=\boldsymbol{d}\otimes\boldsymbol{W}$, $\boldsymbol{d}=[d_0,\ldots,d_{N_f-1}]^T$ with size $N_f\times 1$, and $\otimes$ represents the Kronecker product. We note that there are $N_f\times N_f$ blocks in the first term on the right-hand side of (11) and the identity matrix has dimension MN_cN_f.

Under the Gaussian assumption, the LLF of the received signal $\boldsymbol{r}$ can be written in the following form:

$$L(\boldsymbol{r};\boldsymbol{\theta})=-\underbrace{\boldsymbol{r}^T\boldsymbol{R}_r^{-1}\boldsymbol{r}}_{L_1}-\underbrace{\ln(\det(\boldsymbol{R}_r))}_{L_2} \tag{12}$$

where $\boldsymbol{\theta}=(P_0,\ldots,P_{L-1},D)$ is the vector of unknown parameters, consisting of the APDP values and the integer delay. The dependence of the LLF on $\boldsymbol{\theta}$ is through the covariance matrix, i.e., $\boldsymbol{R}_r\equiv\boldsymbol{R}_r(\boldsymbol{\theta})$ in (11).

After some manipulations, we find that the terms L_1 and L_2 in the right-hand side of (12) are equal to

$$L_1=-\frac{E_p}{\sigma_n^4}\boldsymbol{r}^T\boldsymbol{W}_r\left(\boldsymbol{R}_h^{-1}+\frac{E_pN_f}{\sigma_n^2}\boldsymbol{I}\right)^{-1}\boldsymbol{W}_r^T\boldsymbol{r}+C_1 \tag{13}$$

and

$$L_2=\sum_{l=0}^{L-1}\ln\det\left(\frac{E_pN_f}{\sigma_n^2}\boldsymbol{R}_h+\boldsymbol{I}\right)+C_2 \tag{14}$$

where C_1 and C_2 are constants independent of the unknown parameter vector $\boldsymbol{\theta}$. The inverse of $\boldsymbol{R}_r$, which is needed in L_1, can be obtained with the help of the matrix inversion lemma [22].

In light of (13), it is convenient to define the $L\times 1$ vector $\boldsymbol{z}=(1/N_f)\boldsymbol{W}_r^T\boldsymbol{r}$, whose lth entry can be expressed as

$$z(l;D)=\frac{1}{N_f}\sum_{j=0}^{N_f-1}d_j\boldsymbol{w}_{D+l}^T\boldsymbol{r}_j \tag{15}$$

where the dependence on D is now made explicit. Note that, on the basis of (8), the inner product $\boldsymbol{w}_l^T\boldsymbol{r}_j$ represents the lth output (at the chip rate) of a filter

matched to the transmitted pulse $w(t)$, when applied to the observed data in the jth frame. Accordingly, the vector $\boldsymbol{z}$ contains delayed values (by D) of the matched filter output, further averaged over the N_f available frames.

Making use of (15) and (3) in (13) and after further simplifications, the final expression of the LLF can be obtained as

$$L(\boldsymbol{r};\boldsymbol{\theta}) = \sum_{l=0}^{L-1}\left[\frac{\mathrm{SNR}_l}{(1+\mathrm{SNR}_l)}\frac{z^2(l;D)N_f}{\sigma_n^2} - \ln(1+\mathrm{SNR}_l)\right] \tag{16}$$

where we define

$$\mathrm{SNR}_l = \frac{N_f E_p P_l}{\sigma_n^2}, \quad l=0,1,\ldots,L-1 \tag{17}$$

The latter gives the SNR for the lth propagation path and is a function of the unknown parameter P_l.

The joint ML estimator of the integer delay D and the APDP values P_l, $l=0,\ldots,L-1$, can be obtained by maximizing the log-likelihood function with respect to these parameters. Unfortunately, the large dimension (i.e., $L+1$) of the resulting parameter vector $\boldsymbol{\theta}$ prohibits a practical implementation of this search. In the next section, we develop a simplified scheme based on a lower-dimensional parametric model of the APDP.

3.2. Estimation of average power delay profile

If the APDP was known, one could estimate the TOA via a simple one-dimensional search of the LLF in (16) over the discrete delay parameter D. Motivated by this observation, we propose to first estimate the APDP and then substitute the results back in (16) for the final search. Ideally, as described in Section 2, the APDP of a UWB channel exhibits a double-exponential decay as a function of the excess delay parameter l, as given by (4). Here, we adopt a curve fitting approach based on a weighted least-squares (LS) rule to fit such a model to a function of the observed data. Because of the importance of the single cluster case ($C=1$) in the literature and the resulting simplifications in the APDP estimation, we treat it separately from the multiple clusters ($C>1$) case.

3.2.1. Single cluster fitting

Differentiating (12) with respect to P_l and setting the result to 0, we first obtain a preliminary APDP estimate conditioned on D as follows:

$$\hat{P}_l^{(0)}(D) = \max\left\{\frac{1}{E_p}[z(l;D)^2 - \sigma_N^2], \delta_0\right\}, \quad l=0,\ldots,L-1 \tag{18}$$

where $z(l;D)$ is the time-shifted correlator output (15), δ_0 is a small positive number and the maximum operation is used to ensure that the estimate $\hat{P}_l^{(0)}(D) \geq \delta_0 > 0$ for all l.

For the single cluster model, we seek to fit the calculated $\hat{P}_l^{(0)}(D)$ in (18) to a simplified form of the APDP (4) with only a single exponentially decaying envelope, i.e., $P_l = \beta e^{-l\alpha}$ for $l=0,\ldots,L-1$, with parameters $\alpha>0$ and $\beta>0$. Since an exponential decay in linear scale becomes a straight line in logarithmic scale, we choose to carry out the curve fitting in the log-domain and seek values of α and β that best fit $\ln \hat{P}_l^{(0)}(D)$ in a weighted LS sense. Specifically, these parameters are obtained by solving the following optimization problem:

$$\min_{\alpha,\beta} \sum_{l=0}^{L-1} \mu_l \left|\ln \hat{P}_l^{(0)}(D) - (\ln\beta - l\alpha)\right|^2 \tag{19}$$

where $\mu_l \geq 0$ denotes a suitable weighting sequence. Our use of μ_l and our choice for its specific form have a simple intuitive justification. Ideally, we would like to include in the fitting only the data points that correspond to actual multipath components (MPCs). Also, due to the log operation, we find that paths with very low power would be overemphasized in the objective function, which lead to poor fitting. Therefore, we propose to include in the fitting only the local maxima, as they are more likely to correspond to MPCs, and discard the very low power values at the same time. Accordingly, we set $\mu_l = 1$ if there is a local maximum, i.e., $\hat{P}_{l-1}^{(0)}(D) < \hat{P}_l^{(0)}(D) > \hat{P}_{l+1}^{(0)}(D)$, and 0 otherwise. This approach, which has been confirmed experimentally, allows us to mask out the noisy low power data points, as desired.

The analytic solution to (19) is given by

$$\hat{\alpha} = -\frac{\sum_{l=0}^{L-1}\mu_l(l-A_1)\ln \hat{P}_l^{(0)}(D)}{A_0A_1^2 - A_0A_2} \tag{20}$$

$$\hat{\beta} = \exp\left(\frac{1}{A_0}\sum_{l=0}^{L-1}\mu_l \ln \hat{P}_l^{(0)} + A_1\hat{\alpha}\right) \tag{21}$$

where we define

$$A_0 = \sum_{l=0}^{L-1}\mu_l, \quad A_1 = \frac{1}{A_0}\sum_{l=0}^{L-1} l\mu_l, \quad A_2 = \frac{1}{A_0}\sum_{l=0}^{L-1} l^2\mu_l \tag{22}$$

Note that A_0 is the total number of local maxima, while A_1 and A_2 correspond to the first and second moments of the weighting μ_l respectively.

With the above values of $\hat{\alpha}$ and $\hat{\beta}$, a new APDP estimate is obtained as follows:

$$\hat{P}_l^{(1)}(D) = \hat{\beta}e^{-l\hat{\alpha}}, \quad l=0,\ldots,L-1 \tag{23}$$

This estimate can easily be calculated for every possible D in the range of $1,2,\ldots,D_{max}$, and then substituted back in (16) to finalize the one-dimensional search over the delay parameter, as further discussed in Section 3.3. Although single cluster fitting may lead to an oversimplified description of the overall APDP, its use in connection with the LLF (16) can still provide a fine estimation of the unknown delay D. However, in cases where there are multiple separated clusters in the UWB channel, we find that the TOA performance can be improved by using a more sophisticated fitting approach that better reflects this situation.

3.2.2. Multiple clusters fitting

In this case, we would like to adjust the parameters in the complete model (4) to achieve the best fit with the available data obtained for a specific channel. Since a more complicated APDP model is adopted, it is desirable to estimate its parameters only once; that is, to minimize complexity, we will not seek to estimate a new $\hat{P}_l^{(1)}$ for every possible D.

It turns out that for this purpose, only a rough estimate of D is needed, and this can be obtained by considering the complete set of instantaneous power values at the matched filter output, i.e., $\hat{P}_i^{(0)}(0)$, as given by (18) with $D=0$ but with the range of the subscript i now extended over the entire frame, i.e., $i=0,\ldots,N_c-1$. To obtain the preliminary delay estimate of D, say $\hat{D}_p$, we use a method similar to the maximum energy sum selection (MESS) in [13], with the main difference that a threshold is adopted to rule out impossible timing points. As a result, the search range for the delay is now much smaller, which greatly reduces the computational cost. Based on the estimate $\hat{D}_p$, we form the sequence $\hat{P}_l^{(0)}(\hat{D}_p)$ for $l=0,\ldots,L-1$ and use it to fit the parameters of the multiple cluster model in (4). To this end, we propose an iterative weighted LS approach, which searches for, and fits consecutive clusters one at a time, until a stopping criterion has been met.

A detailed description of the proposed algorithmic steps follows[2]:

*Step*1: We fit the instantaneous log power data for the whole frame (i.e., $\ln \hat{P}_i^{(0)}(0)$, $i=0,\ldots,N_c-1$), to a straight line $l_{TH_1}(i)=\ln\beta-i\alpha$, which will be used as a basic threshold. In particular, the parameters α and β are obtained via a weighted LS fitting similar to (19), but where the range of summation is now from 0 to N_c-1

$$\arg\min_{\alpha,\beta}\sum_{i=0}^{N_c-1}\mu_i\left|\ln\hat{P}_i^{(0)}(0)-(\ln\beta-i\alpha)\right|^2 \tag{24}$$

where $\mu_i=1$ if $\hat{P}_i^{(0)}(0)$ is a local maximum and 0 otherwise. The use of $l_{TH_1}(i)$ will greatly reduce the search range for the preliminary estimate of $\hat{D}_p$ in the next step.

*Step*2: We identify the local maxima of $\ln\hat{P}_i^{(0)}(0)$ which are above the basic threshold line $l_{TH_1}(i)$. Among these local maxima, we consider those in the range $0\le i\le D_{max}$. For each of these points, we calculate the sum $\sum_{l=0}^{L-1}\ln\hat{P}_l^{(0)}(i)$. The value of i for which this sum is maximum is taken as the estimate $\hat{D}_p$. The latter also gives us the position of the first cluster in the frame, i.e., $c_0=\hat{D}_p$.

*Step*3: We fit the local maxima of $\ln\hat{P}_l^{(0)}(\hat{D}_p)$, $l=0,\ldots,L-1$ to a new straight line, denoted by $l_{TH_2}(l)$, using the same procedure as in the single exponential case. This new threshold, obtained using the data of all the clusters, will be used to determine the onset of any new cluster, that is, the APDP value at the starting point of each cluster, given by parameter β_k, should be above $l_{TH_2}(l)$.

*Step*4: We search for new clusters using $l_{TH_2}(l)$ as a threshold. Assuming that the starting time of the current cluster c_k is known, we detect a new cluster if we find at least one point $\hat{P}_l^{(0)}(\hat{D}_p)$ that is above $l_{TH_2}(l)$ in the range $c_k+\lfloor\tau_{mic}/T_c\rfloor\le i\le c_k+L$, where τ_{mic} is the minimum inter-cluster delay depending on the channel environment, e.g., $\tau_{mic}=10$ ns. We denote the corresponding abscissae l for these points as $l_j, j=1,\ldots,J$, where J is the total number of such points.

*Step*5: Once a new cluster is detected, we have to identify its starting time. Intuitively, l_1 could be considered as the new cluster starting time. However, this may not be the best choice due to noise and the random nature of the channel. Therefore, to select the starting time of the new cluster c_{k+1}, we proceed as follows. For each $j=1,\ldots J$, we temporarily set $c_{k+1}=l_j$ and perform a weighted LS fitting of the current exponential cluster between c_k and l_j according to

$$\arg\min_{\alpha_k,\beta_k}\frac{\sum_{i=c_k}^{l_j-1}\mu_i\left|\ln\hat{P}_i^{(0)}(0)-(\ln\beta_k-(i-c_k)\alpha_k)\right|^2}{\sum_{i=c_k}^{l_j-1}\mu_i} \tag{25}$$

The value of l_j with the smallest average LS fitting error is chosen as the new cluster starting time, that is $c_{k+1}=l_j$, and the corresponding values of α_k and β_k are used as model parameters for the current cluster.

*Step*6: We repeat Steps 4 and 5 until there are no new clusters detected and we let C denote the total number of detected clusters.

3.3. TOA estimation

For the single cluster case, we let the estimated $\hat{P}_l^{(1)}(D)$ in (23) depend on the integer delay D. Since we simply assume one decaying exponential, it is simple to calculate this APDP estimate for every possible D. Note that α should be positive to ensure an exponential decay; therefore, tentative delays D that lead to a negative value of α should be discarded. For every possible D in the search range, we substitute $\hat{P}_l^{(1)}(D)$ back into the LLF (16), and then search for the maximum over D, which is the only unknown parameter left to be estimated.

For the multiple clusters case, the APDP estimate $\hat{P}_l^{(1)}$ obtained from the above procedure bears no dependence on D. Inserting the refined APDP estimate $\hat{P}_l^{(1)}$ back into the LLF (16), again, the only unknown parameter left to be estimated is D, which can be finally obtained via a simple one-dimensional integer search. We note that once the APDP has been estimated, the final LLF $L(D)$ only depends on the matched filter outputs $z(l;D)$ and the background noise variance σ_n^2, which can be obtained from *a priori* estimation. We denote the final delay estimate by $\hat{D}$.

3.4. Complexity analysis

The computational complexity of our proposed approach mainly depends on two factors, namely the preliminary LS-based APDP estimation and the subsequent TOA estimation which involves the maximization of the LLF.

For the sake of conciseness, our analysis of the APDP estimation complexity focuses on multiple cluster fitting as in Section 3.2.2. This approach begins in Step 1 with the preliminary calculation of N_c log power values, at cost of $4N_c$ flops.[3] The core of the procedure then relies on the application of multiple LS estimation steps, in which a set

[2] At this point, the reader may consult Fig. 2 for further clarifications on these steps; the experimental methodology for generating this figure will be explained in detail in Section 5.

[3] The computational complexity is evaluated in terms of the number of required floating point operations (flop), where a multiply-add, a division and a numerical function evaluation (e.g., log) each count for one flop.

of power measurements, represented here by a vector $\boldsymbol{b}$ of generic length m, are fitted to a straight line in the log domain, represented by the product $\boldsymbol{Ax}$ where $\boldsymbol{A}$ is a known matrix of size $m\times 2$ and $\boldsymbol{x}=[\alpha,\beta]^T$ is the vector of unknown parameters. The efficient implementation of the LS method then involves the QR factorization of matrix $\boldsymbol{A}$, with a cost of 8 m, followed by the computation of the unknown parameters with a cost of 4 m. Therefore, the total cost for each LS estimation step is 12 m, which is linear in m. In Step 1, we have $m<N_c$, while in Step 3, we have $m<L\le N_c$. For Step 5, it is necessary to perform multiple LS fittings of various sizes. For simplicity, let us assume a constant value of J for each cluster index k. Because the cost of each LS fit is linear in m, it can be verified that the total cost of Step 5 is upper bounded by $12JL$. The total complexity of the multiple cluster APDP estimation algorithm is therefore upper bounded by $16N_c+12(J+1)L$ where J would typically be a small integer. Because we only use local maxima in the fitting, these bounds tend to be very conservative.

For each frame, we assume that the N_c squared correlator values, i.e., $z(l;0)^2$ for $l=0,\ldots,L-1$, are available. For each $l=0,\ldots,L-1$, we first compute the numerical coefficients $a_l=\mathrm{SNR}_l/(1+\mathrm{SNR}_l)$, at the cost of $4L$. From there, each evaluation of the LLF (16) amounts to the calculation of an inner product. The total cost of the ML search is therefore of the order of LD_{max}, where D_{max} delimits the range for the TOA search. This cost for the evaluation and maximization of the LLF is comparable to that of competing sub-Nyquist estimators which, when implemented at the same sampling rate, require the evaluation of an inner product with similar size for each tentative value of the unknown delay [13,14].

In practice, we find that the search range $D_{max}\ge 12J$, so that the total computational cost is dominated by the ML search for the TOA estimation, with the APDP estimation representing only a smaller fraction of the former.

4. Cramer Rao bound

The CRB provides a lower bound on the covariance matrix of any unbiased point estimator of a parameter vector. Specifically, if $\hat{\boldsymbol{\theta}}(\boldsymbol{r})$ denotes such an estimator of vector $\boldsymbol{\theta}=[\theta_0,\ldots,\theta_L]$, we have that

$$\mathrm{Cov}(\hat{\boldsymbol{\theta}}(\boldsymbol{r}))\ge \boldsymbol{J}(\boldsymbol{\theta})^{-1} \tag{26}$$

where $\mathrm{Cov}(\cdot)$ denotes the covariance matrix of its vector argument, and $\boldsymbol{J}(\boldsymbol{\theta})$ is the $L+1$ by $L+1$ Fisher information matrix. The latter is defined in terms of its entries

$$J_{i,j}(\boldsymbol{\theta})=-E\left[\frac{\partial^2 L(\boldsymbol{r};\boldsymbol{\theta})}{\partial\theta_i\partial\theta_j}\right],\quad i,j=0,\ldots,L \tag{27}$$

where the expectation is based on the data model with parameter vector $\boldsymbol{\theta}$. The CRB is of practical interest here since the ML estimator can achieve this bound asymptotically under certain limiting conditions [23]. In this section, we derive the CRB for the joint estimation of the TOA and APDP, as represented by the unknown parameter vector $\boldsymbol{\theta}$.

To simplify the derivations, and especially manipulations involving differentiation with respect to time, we begin by introducing an equivalent integral representation for the discrete sample values at the matched filter output. That is, we let

$$z(l;D)\approx\frac{1}{N_f T_s}\int_0^{T_o} r(t)\xi(t-(l+D)T_c)\,dt \tag{28}$$

where the template signal $\xi(t)$ is defined by

$$\xi(t)=\sum_{j=0}^{N_f-1} d_j w(t-jT_f) \tag{29}$$

This approximation is well justified for small values of T_s, i.e., $T_s\le 1/2B$ as previously assumed.

We differentiate (16) with respect to P_l and D, to obtain

$$\begin{aligned}\frac{\partial L(\boldsymbol{r};\boldsymbol{\theta})}{\partial P_l}&=\frac{\partial L(\boldsymbol{r};\boldsymbol{\theta})}{\partial \mathrm{SNR}_l}\frac{\partial \mathrm{SNR}_l}{\partial P_l}\\&=\frac{E_p N_f}{\sigma_n^2(1+\mathrm{SNR}_l)}\left[\frac{z^2(l;D)N_f}{\sigma_n^2(1+\mathrm{SNR}_l)}-1\right]\end{aligned} \tag{30}$$

and

$$\frac{\partial L(\boldsymbol{r};\boldsymbol{\theta})}{\partial D}=\frac{2N_f}{\sigma_n^2}\sum_{l=0}^{L-1}\frac{\mathrm{SNR}_l}{1+\mathrm{SNR}_l}z(l;D)z'(l;D) \tag{31}$$

where we define

$$z'(l;D)=\frac{\partial z(l;D)}{\partial D}=-\frac{M}{N_f}\int_0^{T_0} r(t)\xi'(t-(l+D)T_c)\,dt \tag{32}$$

and

$$\xi'(t)=\frac{d\xi(t)}{dt} \tag{33}$$

Based on (30) and (31), we can further obtain the required second order derivatives

$$-E\left[\frac{\partial^2 L(\boldsymbol{r};\boldsymbol{\theta})}{\partial P_{l_1}\partial P_{l_2}}\right]=0\quad \forall l_1\ne l_2 \tag{34}$$

$$-E\left[\frac{\partial^2 L(\boldsymbol{r};\boldsymbol{\theta})}{\partial P_l^2}\right]=\frac{E_p^2}{(E_p P_l+\sigma_n^2/N_f)^2}\left(\frac{2E[z(l;D)^2]}{E_p P_l+\sigma_n^2/N_f}-1\right) \tag{35}$$

$$-E\left[\frac{\partial^2 L(\boldsymbol{r};\boldsymbol{\theta})}{\partial P_l\partial D}\right]=-\frac{2E_p N_f^2}{\sigma_n^4}\frac{E[z(l;D)z'(l;D)]}{(1+\mathrm{SNR}_l)^2} \tag{36}$$

and

$$E\left[\frac{\partial^2 L(\boldsymbol{r};\boldsymbol{\theta})}{\partial^2 D}\right]=-\frac{2N_f}{\sigma_n^2}\sum_{l=0}^{L-1}\frac{\mathrm{SNR}_l}{1+\mathrm{SNR}_l}(E[z(l;D)z''(l;D)]+E[z'(l;D)^2]) \tag{37}$$

Next, to calculate (35)–(37), we need to evaluate the expected values $E[z(l;D)^2]$, $E[z(l;D)z'(l;D)]$ and $E[z(l;D)z''(l;D)+z'(l;D)^2]$ at the true value of D.

For the transmitted pulse, since $w(T_c)=w(0)=0$ is the common case in practice, it comes naturally that

$$\int_0^{T_c}\frac{dw(t)}{dt}w(t)\,dt=\frac{1}{2}[w^2(T_c)-w^2(0)]=0 \tag{38}$$

and therefore

$$\int_0^{T_c}\frac{d^2w(t)}{dt^2}w(t)\,dt=-\int_0^{T_c}\left(\frac{dw(t)}{dt}\right)^2 dt \tag{39}$$

After some manipulations using the (38) and (39), the required expectations in (35)–(37) can be obtained as follows:

$$E[z(l;D)^2] = E_p P_l + \frac{\sigma_n^2}{N_f} \tag{40}$$

$$E[z(l;D)z'(l;D)] = 0 \tag{41}$$

and

$$E\{z(l;D)z''(l;D) + z'(l;D)^2\} = -\gamma E_p P_l T_c^2 \tag{42}$$

where the parameter

$$\gamma = \frac{\int_0^{T_c} (dw(t)/dt)^2\, dt}{\int_0^{T_c} w(t)^2\, dt} \tag{43}$$

is positive and determined by the pulse shape.

Based on (36) and (41), it follows that:

$$-E\left\{\frac{\partial^2 L(\boldsymbol{r};\boldsymbol{\theta})}{\partial P_l \partial D}\right\} = 0 \quad \forall l \tag{44}$$

Together with (34), this implies that the Fisher information matrix $\boldsymbol{J}(\boldsymbol{\theta})$ is diagonal. Using (35), (37), (40) and (42), the diagonal entries of $\boldsymbol{J}(\boldsymbol{\theta})$ can be obtained as

$$J_{l,l} = -E\left\{\frac{\partial^2 L(\boldsymbol{r};\boldsymbol{\theta})}{\partial^2 P_l}\right\} = \left[\frac{E_p N_f}{\sigma_n^2(1+\mathrm{SNR}_l)}\right]^2, \quad l = 0,\ldots,L-1 \tag{45}$$

and

$$J_{L,L} = -E\left[\frac{\partial^2 L(\boldsymbol{r};\boldsymbol{\theta})}{\partial^2 D}\right] = \frac{2\gamma E_p N_f T_c^2}{\sigma_n^2} \sum_{l=0}^{L-1} P_l \frac{\mathrm{SNR}_l}{1+\mathrm{SNR}_l} \tag{46}$$

Consequently, the CRBs are given by

$$\mathrm{Var}(\hat{P}_l) \geq J_{l,l}^{-1} = P_l^2 \left(1 + \frac{1}{\mathrm{SNR}_l}\right)^2 \tag{47}$$

$$\mathrm{Var}(\hat{D}) \geq J_{L,L}^{-1} = \frac{1}{2\gamma T_c^2} \left(\sum_{l=0}^{L-1} \frac{\mathrm{SNR}_l^2}{1+\mathrm{SNR}_l}\right)^{-1} \tag{48}$$

From the formulas in (47) and (48), it is obvious that the CRBs depend on the SNR_l. When $\mathrm{SNR}_l \gg 1$, the expressions for the CRB take simplified forms as follows:

$$\mathrm{Var}(\hat{P}_l) \geq J_{l,l}^{-1} \approx P_l^2 \tag{49}$$

and

$$\mathrm{Var}(\hat{D}) \geq J_{L,L}^{-1} \approx \frac{\sigma_n^2}{2(\sum_{l=0}^{L-1} P_l)\gamma E_p N_f T_c^2} \tag{50}$$

Consequently, the CRB for the TOA estimate $\hat{\tau}$ becomes

$$\mathrm{Var}(\hat{\tau}) \geq \frac{\sigma_n^2}{(\sum_{l=0}^{L-1} P_l) 2\gamma E_p N_f} \tag{51}$$

We note from (49) that the standard deviation for the APDP at the lth tap is lower bounded by the corresponding power value, which is consistent with well-known results from the theory of unsmoothed power profile estimation [24]. Lower bounds on the estimation variance of the APDP parameters α_k and β_k can be obtained in turn by applying the chain rule for derivatives to (27) and making use of the results in (34) and (45). As for the CRB of the TOA in (51), it is inversely proportional to the total average power over the L taps, i.e., $\sum_{l=0}^{L-1} P_l$, the ratio of pulse energy-to-noise variance E_p/σ_n^2, the pulse shape factor γ in (43) and the number of frames N_f.

5. Simulation and results

5.1. Methodology

In the simulations carried out here, the frame duration is set to T_f=200 ns; each frame is further divided into N_c=400 chips of duration T_c=0.5 ns. Unless specified otherwise, the number of transmitted frames is set to N_f=60. It is also assumed that each frame is equivalent to a single symbol. The transmitted UWB pulse $w(t)$ is a unit-energy Gaussian doublet [25] with duration T_c and effective bandwidth B=4 GHz. The energy per pulse E_p is given in terms of the SNR parameter E_p/σ_n^2. The assembled pulse sequence is then filtered by a multipath UWB channel.

The channel impulse responses used in our work are derived from the IEEE 802.15.4a typical channel models [15]. These impulse responses are randomly generated such that the multipath arrival times are grouped into multiple clusters, each cluster being characterized by an exponentially decaying average power envelope. Several such models have been developed to fairly represent channel conditions in different types of environments, such as residential, office, outdoor and industrial settings. The parameters of these models have been adjusted based on measurements over a representative range of frequencies and distances.

As mentioned in Section 3, the single cluster fitting method utilizes the overall fading of the channel with delay by assuming a single exponentially decaying profile; therefore, this simple method can be applied to all kinds of realistic channels. The multi-cluster fitting method seeks to further exploit finer details present in the APDP structure, i.e., by representing it in terms of multiple exponentially decaying components caused by the physical environment. When there is a clear multi-cluster structure in the channel, this method will indeed lead to better performance than the previous one. We note that the multi-cluster structure is very common for indoor UWB channels, as indicated by the measurement results in [5].

In our experiments, minor modifications were made to these IEEE channel models to allow for explicit control of the APDP parameters, i.e., number of clusters C, and for each cluster, shape parameters α_k,β_k,c_k. The results presented next focus on the CM3 channel model, which is representative of an indoor office environment; however, similar results and conclusions were obtained with other standard channels. The following parameter values were used: delay spread τ_{ds} = 120 ns, number of taps L=240 and maximum delay τ_{max} = 80 ns. We note that the tap spacing of the created channel can be smaller than T_c, while our method still works fine with the assumption of T_c spaced taps.

Zero-mean white noise is added to the time domain samples at the UWB channel output. At the receiver side, the baseband antenna signal is passed through a (digital) filter matched to a local copy of the transmitted reference

$s(t)$. The MF output is then sampled at the sub-Nyquist rate $1/T_c$ and the resulting samples are used in the ML estimator of τ and P_l as explained in Section 3. In addition, several TOA estimators from the recent literature are implemented and used as benchmarks.

The TOA estimation performance is evaluated in terms of the root mean square error (RMSE), defined as $\sqrt{E[(\hat{D}T_c-\tau_0)^2]}$ where $\hat{D}$ and τ_0 denote the estimated integer delay and the true value of the delay, respectively. In the Monte-Carlo simulations, the RMSE is approximated by averaging over 1000 independent channel trials, where in each trial a different value of τ_0 is selected randomly from the interval $(0,\tau_{max}]$. That is, τ_0 here is arbitrary and not limited to being an integer multiple of T_c.

5.2. Results and discussion

The fitting in semi-logarithmic scale for several clusters is illustrated in Fig. 2 for a particular set of observed data with SNR=30 dB, as obtained with a CM3 channel displaying three identifiable clusters in its APDP structure. The longest straight line is the basic threshold $l_{TH_1}(i)$, which helps to select the first preliminary estimate $\hat{D}_p$ and the corresponding log values $\ln \hat{P}_l^{(0)}(\hat{D}_p)$, $l=0,\ldots,L-1$. The second longest straight line represents the new threshold $l_{TH_2}(l)$, that is used in turn to detect the clusters. Finally, the $C=3$ clusters detected in this example are fitted using the three shorter straight lines of varying slopes.

After getting all the needed parameters, i.e., C and the set of triplets $\{\alpha_k,\beta_k,c_k\}_{k=0}^{C-1}$, the final APDP estimate $\hat{P}_l^{(1)}$ can be calculated according to the general expression in (4). The newly estimated APDP $\hat{P}_l^{(1)}$ is plotted in linear scale in Fig. 3, along with the true APDP P_l based on the exact parameter values. It is seen that the proposed method provides a sufficiently accurate estimation of the true APDP. In this figure, we also show the result of single cluster estimation, showing that the single cluster method can be used to provide useful information about the rate of decay of the APDP even in this case.

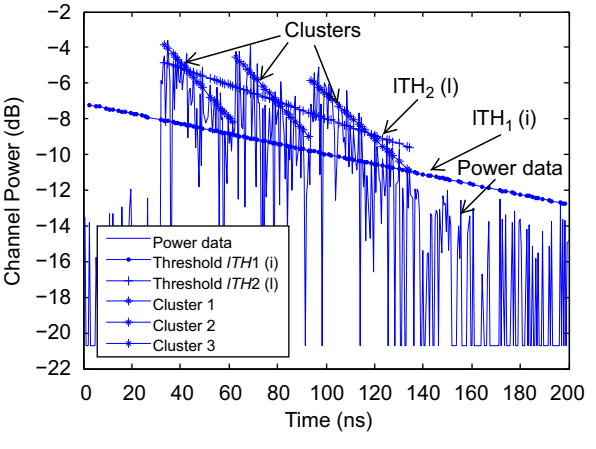

Fig. 2. Comparison of APDP fitting to raw power data in log scale (SNR=30 dB).

To see whether multi-cluster fitting offers any performance advantages over single-cluster fitting, we compared the average fitting error and final TOA estimation performance as a function of the assumed number of clusters. For each experimental trial, we generate TOA estimates corresponding to different numbers of clusters, specifically: fixing $C=1$, 2 and 3. For each of the considered cases, we show in Fig. 4 the average fitting error (defined by $\sum_{l=0}^{L-1}\mu_l|\hat{P}_l^{(0)}-\hat{P}_l^{(1)}|^2/\sum_{l=0}^{L-1}\mu_l$) as a function of the SNR. It can be seen that multi-cluster fitting yields the lowest fitting error, followed by 2-cluster fitting and 1-cluster fitting.

In Fig. 5 we show the corresponding RMSE of TOA estimation. The same trend as in Fig. 4 is observed where it is seen that multi-cluster fitting also yields the best TOA estimation performance. It is interesting that while the variations in the average fitting errors are relatively small, the gain in TOA performance can be significant, especially in the mid to high SNR range, i.e., between 15 dB and 30 dB, which is of great practical interest.

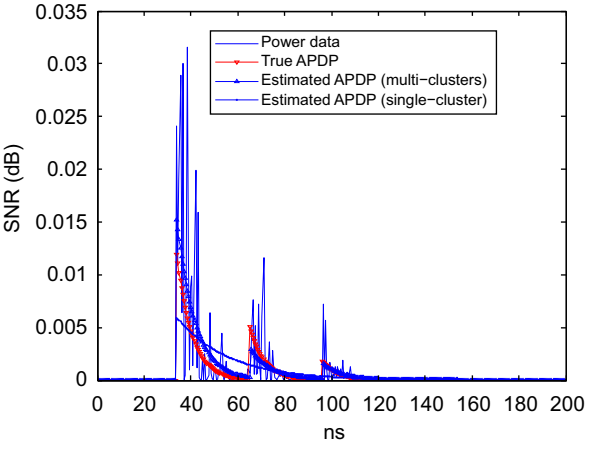

Fig. 3. Comparison of estimated and true APDP in linear scale (SNR=30 dB).

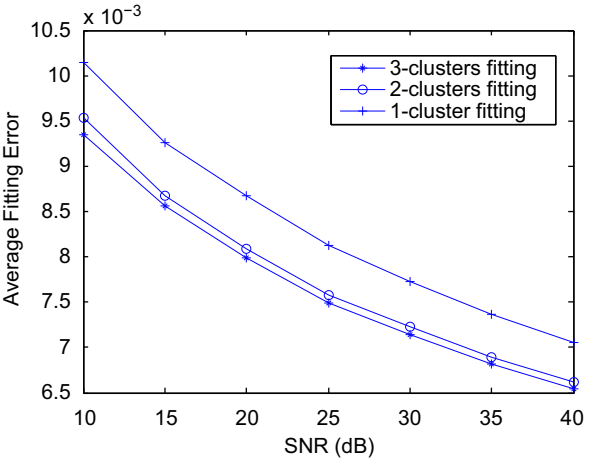

Fig. 4. Average APDP fitting error versus SNR .

Fig. 6 shows the TOA estimation performance of the proposed multi-cluster fitting-based method as a function of the SNR for different values of the number of frames N_f. As expected, the TOA estimation accuracy improves as the number of frames increases, due to the averaging operation that reduces the effect of noise.

Next, we compare the proposed TOA estimator with the WMESS, DW-MESS [13] and ML with partial channel information (MLP) [14] estimators. Since these methods require *a priori* knowledge of the APDP, we evaluate their performance with the true APDP (used to generate the CM3 channels) and with the estimated APDP obtained using the proposed multi-cluster method in Section 3.2. For a fair comparison, all the methods use the same sub-Nyquist sampling period of 0.5 ns. The window length for the reference methods is set to 120 ns, which is equal to the channel delay spread τ_{ds}. The other parameter values are the same as for the proposed method. Fig. 7 shows the performance of the four methods under consideration as a function of the SNR. We can see that the proposed method achieves a better accuracy than the previously proposed methods when the latter use the estimated APDP. Even when they use the true APDP, the proposed method outperforms WMESS and performs closely to the other two methods at high SNR.

We also investigate the behavior of the proposed approach under low levels of IFI. To this end, we consider an extended version of the CM5 channel model of total duration $\tau_{ds} = 280$ ns, which now exceeds the frame duration $T_f = 200$ ns. The tail portion of the response that extends over the next frame, consisting of the paths with delay in excess of 120 ns, is linearly scaled so that its energy $\mathcal{E}_2$ is equal to a given percentage of the energy $\mathcal{E}_1$ within the frame, as represented by $\rho = \mathcal{E}_2/\mathcal{E}_1$. The comparative results obtained with the various sub-Nyquist TOA estimators under consideration in this study, are presented in Fig. 8, which shows the RMSE of the TOA estimates as a function of ρ at an operating SNR of 25 dB. If the level of IFI level is not too large, all the sub-Nyquist estimators can still work properly and maintain the same, or a slightly degraded level of performance. However, when the IFI becomes too large, all the TOA estimators will degrade significantly.

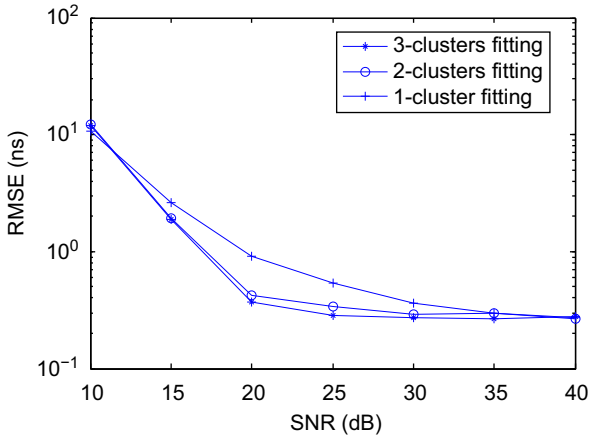

Fig. 5. RMSE of proposed TOA estimator for different (assumed) number of clusters.

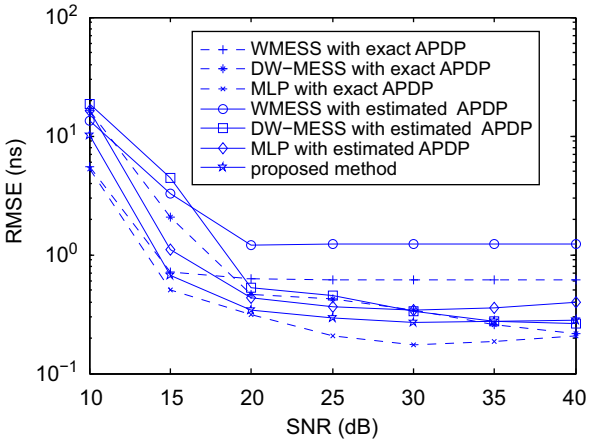

Fig. 7. RMSE of TOA estimates for different algorithms.

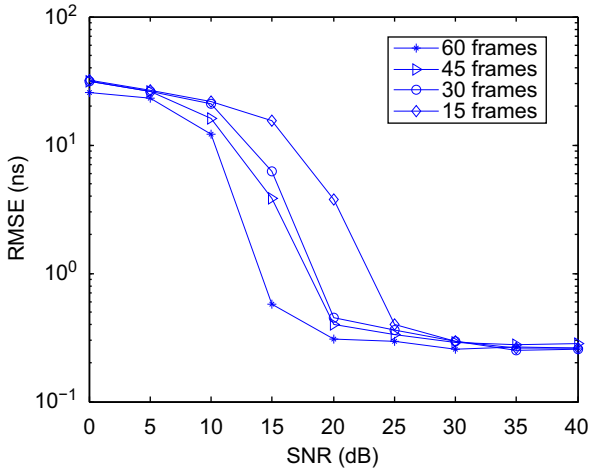

Fig. 6. RMSE of proposed TOA estimator for different number of frames.

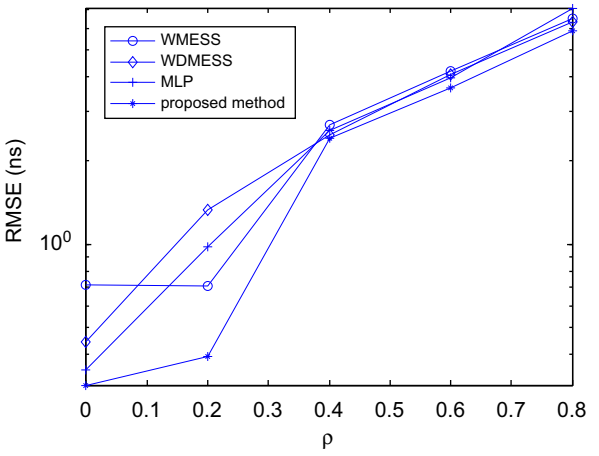

Fig. 8. RMSE of TOA estimation with IFI (SNR=25 dB).

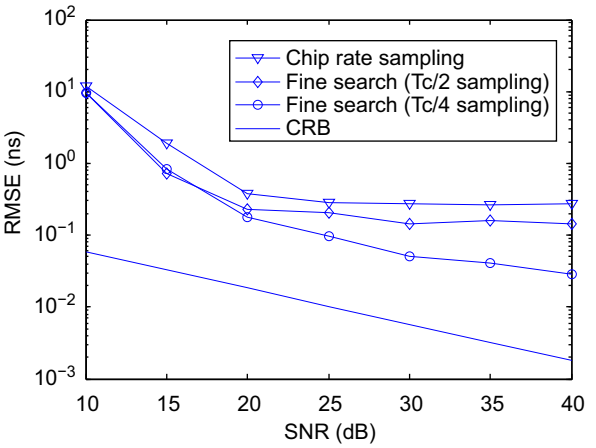

Fig. 9. RMSE of proposed TOA estimator for different sampling rates.

Finally, Fig. 9 compares the RMSE performance of the proposed TOA estimator as a function of the SNR when different time resolutions are used to obtain a finer estimate by searching around the initial estimate $\hat{D}T_c$. The CRB for TOA estimation derived in Section 5 is also shown for reference. From this figure, we conclude that conducting a fine local search using a higher sampling rate can significantly improve the estimation performance. However, this improvement comes at a slightly higher implementation cost.

6. Conclusion

We proposed and investigated a joint sub-Nyquist ML-based estimator of the TOA and APDP to UWB impulse radio applications. A parametric model was assumed for the APDP and its parameters were estimated jointly with the unknown TOA by exploiting the interplay between the ML and LS approaches. This is in contrast to the previous sub-Nyquist methods which require *a priori* knowledge of the APDP. Through simulations, we showed that the proposed TOA estimator has a good accuracy and can outperform earlier methods when using the same estimated APDP. While the joint estimation of the APDP adds to the complexity, the increase is still reasonable since all digital processing is done at the lower chip (sub-Nyquist) rate. The accuracy of the proposed TOA estimator could be improved by fine search with a higher sampling rate.

References

[1] R. Want, An introduction to RFID technology, IEEE Pervasive Computing 5 (2006) 25–33.
[2] C. Xu, C.L. Law, TOA estimator for UWB backscattering RFID system with clutter suppression capability, EURASIP Journal on Wireless Communications and Networking (2010) 14. http://10.1155/2010/753129.
[3] D. Dardari, A. Conti, U. Ferner, A. Giorgetti, M. Win, Ranging with ultrawide bandwidth signals in multipath environments, Proceedings of the IEEE 97 (2009) 404–426.
[4] Z. Sahinoglu, S. Gezici, I. Güvenc, Ultra-wideband Positioning Systems: Theoretical Limits, Ranging Algorithms, and Protocols, Cambridge University Press, 2008.
[5] U. Schuster, H. Bolcskei, Ultrawideband channel modeling on the basis of information-theoretic criteria, IEEE Transactions on Wireless Communications 6 (2007) 2464–2475.
[6] D. Dardari, M. Win, Threshold-based time-of-arrival estimators in UWB dense multipath channels, in: Proceedings of the IEEE International Conference on Communications, 2006, pp. 4723–4728.
[7] M. Win, R. Scholtz, Characterization of ultra-wide bandwidth wireless indoor channels: a communication-theoretic view, IEEE Journal on Selected Areas in Communications 20 (2002) 1613–1627.
[8] K. Liu, H. Yin, C.W., Low complexity tri-level sampling receiver design for UWB time of arrival estimation, in: Time-of-arrival Estimation of UWB Signals in the Presence of Narrowband and Wideband Interference, 2011, pp. 1–5.
[9] J. Lee, R. Scholtz, Ranging in a dense multipath environment using an UWB radio link, IEEE Journal on Selected Areas in Communications 20 (2002) 1677–1683.
[10] S. Gezici, Z. Sahinoglu, A. Molisch, H. Kobayashi, H. Poor, Two-step time of arrival estimation for pulse-based ultra-wideband systems, EURASIP Journal on Advances in Signal Processing (2008) 11. http://dx.doi.org/10.1155/2008/529134.
[11] D. Dardari, C.-C. Chong, M. Win, Threshold-based time-of-arrival estimators in UWB dense multipath channels, IEEE Transaction on Communications 56 (2008) 1366–1378.
[12] J. Youssef, B. Denis, C. Godin, S. Lesecq, New TOA estimators within energy-based receivers under realistic UWB channel statistics, in: Proceedings of the IEEE Vehicular Technology Conference Spring, Taipei, 2010, pp. 1–5.
[13] I. Güvenc, S. Gezici, Z. Sahinoglu, Ultra-wideband range estimation: theoretical limits and practical algorithms, in: Proceedings of the IEEE International Conference on Ultra-Wideband, vol. 3, Hannover, 2008, pp. 93–96.
[14] H. Luecken, C. Steiner, A. Wittneben, ML timing estimation for generalized UWB-IR energy detection receivers, in: Proceedings of the IEEE International Conference on Ultra-Wideband, Vancouver, 2009, pp. 829–833.
[15] A. Molisch, K. Balakrishnan, C. Chong, S. Emami, A. Fort, J. Karedal, J. Kunisch, H. Schantz, U. Schuster, K. Siwiak, IEEE 802.15.4a channel model-final report, IEEE 802.15 WPAN Low Rate Alternative PHY Task Group 4a (TG4a) (2004).
[16] Z. Sahinoglu, S. Gezici, Ranging in the IEEE 802.15.4a standard, in: Proceedings of the IEEE Annual Wireless and Microwave Technology Conference, 2006, pp. 1–5.
[17] D. Dardari, G.A., W.M.Z., Time-of-arrival estimation of UWB signals in the presence of narrowband and wideband interference, in: Proceedings of the IEEE International Conference on Ultra-Wideband, 2007, pp. 1–6.
[18] F. Vanhaverbeke, Y. Guan, M. Moeneclaey, Optimal channel and time-of-arrival estimation for ir-uwb in the presence of pulse overlap, in: Proceedings of the IEEE International Conference on Communications, 2010, pp. 1–5.
[19] Z. Xu, B. Sadler, Time delay estimation bounds in convolutive random channels, IEEE Journal of Selected Topics in Signal Processing 1 (2007) 418–430.
[20] D. Cassioli, M. Win, A. Molisch, The ultra-wide bandwidth indoor channel: from statistical model to simulations, IEEE Journal on Selected Areas in Communications 20 (2002) 1247–1257.
[21] K. Makaratat, T. Brown, S. Stavrou, Estimation of time of arrival of UWB multipath clusters through a spatial correlation technique, IET Microwaves, Antennas and Propagation 1 (2007) 666–673.
[22] D.S. Bernstein, Matrix Mathematics: Theory, Facts, and Formulas, second ed. Princeton University Press, 2009.
[23] H. Poor, An Introduction to Signal Detection and Estimation, Springer-Verlag, New York, 1994.
[24] S.M. Kay, Modern Spectral Estimation: Theory and Practice, Prentice Hall, 1999.
[25] M.D. Benedetto, G. Giancola, Understanding Ultra Wide Band Radio Fundamentals, Prentice Hall, 2004.